Prediction of Channel Excess Attenuation for Satellite Communication Systems at *Q*-Band Using Artificial Neural Network

Lu Bai, Cheng-Xiang Wang, *Fellow, IEEE*, Qian Xu, Spiros Ventouras, and George Goussetis, *Senior Member, IEEE*

***Abstract*—This letter proposes the use of an artificial neural network (ANN) for estimating the fading of a *Q*-band (39.402 GHz) satellite channel exploiting the knowledge of its previous state, as well as the present weather conditions. The ANN is trained using weather data and propagation measurements at the *Q*-band obtained during a period of nine months by the Aldo Paraboni receivers of RAL Space, Chilbolton, Hampshire, U.K. Subsequently, the estimation obtained by the ANN is compared with actual propagation measurements on data obtained over a period of three months. Statistical analysis demonstrates an agreement between the ANN estimation and the measurement within a 1 dB range with a probability exceeding 98.8%. The significance of this letter lies with the opportunities it raises to deliver real-time fading estimations using low-cost weather sensors combined with feedback on the channel state from the return link, which can be used in the deployment of propagation impairment mitigation techniques.**

***Index Terms*—Artificial neural network (ANN), channel excess attenuation, satellite communication systems, weather conditions.**

I. Introduction

THE role of satellite communications in emerging wireless communication systems stems from their capability to deliver worldwide broadband coverage [1]. While traditional satellite services have relied on *C*- and *Ku*-bands, the transition from broadcast to broadband services and the ever-increasing need for higher bandwidth at reduced costs drives the exploitation of higher millimeter-wave (mmW) bands. Currently, the use of the *Q*/*V*-band for the feeder link of satellite communication systems is being rolled out as a means to free *Ka*-band spectrum to revenue generating user links and reduce the per-bit cost of the ground segment [2].

Despite aforementioned advantages, atmospheric fading at the *Q*/*V*-band is significantly higher compared to that at the *C*- or *Ku*-band. Consequently, the traditional approach of allowing for a sufficiently high margin in the link budget is no longer efficient within the existing technology base. Instead, alternative fade mitigation techniques are preferred, such as adaptive coding and modulation and dynamic power control [3], [4]. Critically, the efficient deployment of these techniques relies on the accurate real-time knowledge of the channel fading that will enable the optimum reconfiguration of link parameters, such as the modulation and coding rate, or the power amplifier's input backoff [5], [6].

The attenuation impairments in the tropospheric layer models of satellite communication channels above 10 GHz, such as free-space attenuation, atmospheric gases attenuation, rain attenuation, and clouds and fog attenuation, were considered in [7]–[10], respectively. However, these channel models offered by International Telecommunication Union in [7]–[10] need too much input information for calculation of attenuation impairments and, therefore, are too complex despite the accuracy. By contrast, stochastic models [11]–[15] are easy to use [16], [17]. Aforementioned models were generated by conventional channel modeling methods. They can describe channel characteristics, but cannot accurately predict the received signal attenuation in a certain time resulting from channel impairments. Recently, artificial neural networks (ANNs) widely used in various research areas were shown to have good performance on channel characteristics prediction [18], [19]. In principle, the channel state information (CSI) for broadband services can be reported to the gateway by virtue of the return link. However, the nonnegligible latency associated with the combined forward and return links imposes a delay in the knowledge of the CSI. Additional instrumentation should then be deployed in order to enable real-time estimation of the fading. This includes space-borne beacons with associated ground receivers or radiometers,

Manuscript received March 17, 2019; revised May 22, 2019 and June 7, 2019; accepted June 28, 2019. Date of publication August 2, 2019; date of current version November 4, 2019. This work was supported in part by the National Key R&D Program of China under Grant 2018YFB1801101, in part by the Fundamental Research Funds for the Central Universities under Grant 2242019R30001, in part by the Taishan Scholar Program of Shandong Province, in part by the EU H2020 RISE TESTBED Project under Grant 734325, in part by the Engineering and Physical Sciences Research Council (EPSRC) TOUCAN Project under Grant EP/L020009/1, in part by the EPSRC U.K. under Grant EP/P025129/1, and in part by the EU H2020 ITN REVOLVE project under Grant 722840. *(Corresponding author: Cheng-Xiang Wang.)*

L. Bai is with the Shandong Provincial Key Laboratory of Wireless Communication Technologies, School of Information Science and Engineering, Shandong University, Qingdao 266237, China (e-mail: bailusdu@126.com).

C.-X. Wang is with the National Mobile Communications Research Laboratory, School of Information Science and Engineering, Southeast University, Nanjing 210096, China, also with Purple Mountain Laboratories, Nanjing 211111, China, and also with the Institute of Sensors, Signals and Systems, School of Engineering and Physical Sciences, Heriot-Watt University, Edinburgh EH14 4AS, U.K. (e-mail: chxwang@seu.edu.cn).

Q. Xu is with the School of Computer Science and Technology, Jilin University, Changchun 130012, China (e-mail: quincyxu@hotmail.com).

S. Ventouras is with the STFC Rutherford Appleton Laboratory, RAL Space, Oxford OX11 0QX, U.K. (e-mail: spiros.ventouras@stfc.ac.uk).

G. Goussetis is with the Institute of Sensors, Signals and Systems, School of Engineering and Physical Sciences, Heriot-Watt University, Edinburgh EH14 4AS, U.K. (e-mail: g.goussetis@hw.ac.uk).

Digital Object Identifier 10.1109/LAWP.2019.2932904

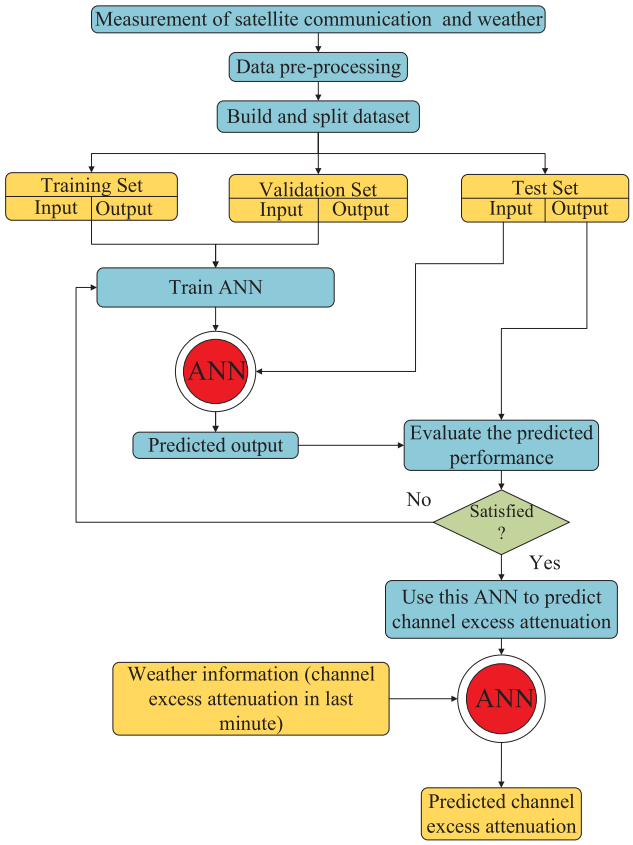

Fig. 1. Flowchart of the channel excess attenuation predicting procedure.

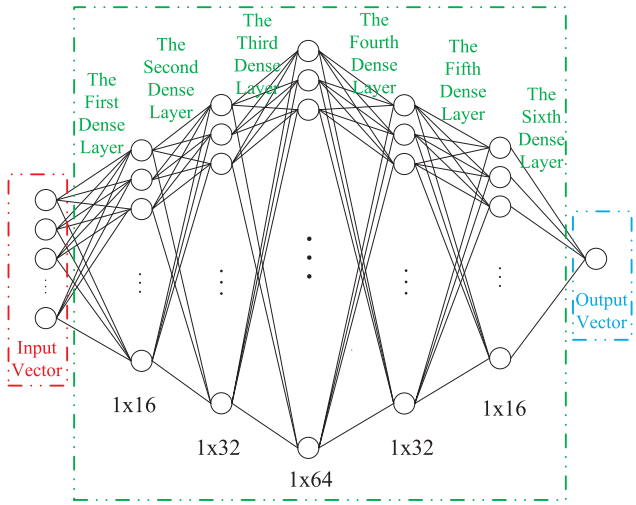

Fig. 2. Architecture of the proposed ANN for channel excess attenuation prediction.

which provide a calibrated reading of the atmosphere's brightness temperature. However, these provisions add a nonnegligible value to the overall costs.

Addressing aforementioned needs, this letter proposes a cost-efficient methodology to obtain the real-time estimation of the atmospheric fading. The proposed approach exploits an ANN, which takes as input earlier fading values, which can be obtained from the return link, as well as the present weather information, which can be obtained from low-cost weather stations. Exploiting Q-band propagation and weather data obtained during a period of one year by the RAL Space Aldo Paraboni Receiver Station in Chilbolton, Hampshire, U.K. [20], we demonstrate that once training has been undertaken, the ANN can then provide an accurate estimation of the real-time fading.

II. System Model

The flowchart of the ANN-enabled approach we adopted for predicting channel excess attenuation associated with a satellite link is shown in Fig. 1. Exploiting the Aldo Paraboni Q-band beacon, we first record the excess attenuation associated with the channel. Together, we also record local weather conditions. The data are then split into three datasets, for training, validation, and testing, respectively. We used the data recorded over a period of one year and split them in the three datasets following a proportion of 2:1:1. The training and validation datasets, both containing input and output vectors, are used to train the network for the parameter selection and configuration of the neural network [21]. When the training process is finished, the input vectors of the test dataset are put into the trained ANN to get the predicted channel excess attenuation. The predicted performance of the trained ANN is evaluated by comparing the predicted channel excess attenuation and the output vectors of the test dataset (i.e., the true measured value).

The architecture of the proposed ANN for predicting the channel excess attenuation is presented in Fig. 2. The output vector Y is the present channel excess attenuation h. In order to evaluate the significance of each input parameter, we explore four different variations of the input vectors, i.e., X_1, X_2, X_3, and X_4, which can be expressed as

$$X_1 = [\alpha, \beta, \gamma, \vartheta, \varphi] \tag{1}$$

$$X_2 = [\alpha, \beta, \gamma, \vartheta, \varphi, h^{'}] \tag{2}$$

$$X_3 = [\alpha, \beta, \gamma, \vartheta, \varphi, \varepsilon, \kappa] \tag{3}$$

$$X_4 = [\alpha, \beta, \gamma, \vartheta, \varphi, \varepsilon, \kappa, h^{'}] \tag{4}$$

$$Y = [h] \tag{5}$$

where $\alpha, \beta, \gamma, \vartheta, \varphi, \varepsilon,$ and κ are the present value for air temperature, relative humidity, rainfall rate, visibility, thickness of rainfall amount, average particle diameter, and average particle speed, respectively, and $h^{'}$ is the channel excess attenuation in the previous 1 min.

The vector X_1 consists of five typical parameters of current weather conditions that can be obtained with low-cost standard instrumentation, namely, air temperature, relative humidity, rainfall rate, visibility, and thickness of rainfall amount. The variable X_3 includes two further parameters that would require the deployment of an additional instrument, a disdrometer, namely, average particle diameter and average particle speed. The comparison between the predicted performance obtained from X_1 and X_3 is meaningful to analyze the significance of deploying a disdrometer. The variables X_2 and X_4 add the

TABLE I
NUMBERS AND PERCENTAGES OF PARAMETERS OF FOUR MODELS

Layers	A model $X_1 \rightarrow Y$		B model $X_2 \rightarrow Y$		C model $X_3 \rightarrow Y$		D model $X_4 \rightarrow Y$	
	Number	Percentage	Number	Percentage	Number	Percentage	Number	Percentage
First dense layer	80	1.53%	96	1.83%	112	2.13%	128	2.43%
Second dense layer	512	9.82%	512	9.79%	512	9.76%	512	9.73%
Third dense layer	2048	39.26%	2048	39.14%	2048	39.02%	2048	38.91%
Fourth dense layer	2048	39.26%	2048	39.14%	2048	39.02%	2048	38.91%
Fifth dense layer	512	9.82%	512	9.79%	512	9.76%	512	9.73%
Sixth dense layer	16	0.31%	16	0.31%	16	0.30%	16	0.30%
Total	5216		5232		5248		5264	

channel excess attenuation recorded in the previous 1 min on X_1 and X_3, which can be obtained exploiting the return link.

After having tested different kinds of ANN architectures and adjusted the architecture parameters of the above ANNs, such as the learning rate, mini batch, epochs, and loss function, the ANN we employed is a multilayer perceptron, which is composed of six dense layers. The six dense layers have 16, 32, 64, 32, 16, and 1 neurons, respectively. Its architecture is shown in Fig. 2. Through iterations using the training dataset, the neural network converges to fit the thresholds, nodes, and weights of connections for the least loss. As shown in Table I, the four models A–D whose input vectors are X_1, X_2, X_3, and X_4 have 5216, 5232, 5248, and 5264 parameters in total, respectively. The third and fourth dense layers have the majority of model parameters, which account for approximately 80% of the total number of model parameters. The loss function is a quantification to evaluate how good a prediction model is in terms of predicting the expected outcome. The mean square error (MSE), which is expressed as R, is the most commonly used regression loss function and easy to use in our multilayer perceptron. It is the average value of squared distances between our target variable and predicted values and can be expressed as

$$R = \frac{\sum_{n=1}^{N}(y_n - y_n^{\mathrm{p}})^2}{N} \tag{6}$$

where N denotes the data numbers of dataset, and y_n and y_n^{p} are the true and predicted values, respectively.

The learning rates for all the dense layers were initialized at 0.0001. The root-mean-square propagation is used to optimize the weights of our multilayer perceptron with the smooth factor of 10^{-6} and the momentum of 0.9. The update rule for weight β is defined as

$$E[g^2]_t = 0.9E[g^2]_{t-1} + 0.1g_t^2 \tag{7}$$

$$\beta_{t+1} = \beta_t - \frac{\eta}{\sqrt{E[g^2]_t + \kappa}} g_t \tag{8}$$

where t, η, and κ denote the iteration index, the learning rate, and the smooth factor, respectively, and g_t is the gradient of the current iteration t [21], [22].

The Xavier uniform initializer, which is also recognized as the Glorot uniform initializer, is applied to initialize the weights in each layer [23]. The weight was generated with a uniform distribution randomly within $[-\varepsilon, \varepsilon]$, where

$$\varepsilon = \sqrt{\frac{6}{\iota_{\mathrm{in}} + \iota_{\mathrm{out}}}} \tag{9}$$

where ι_{in} and ι_{out} are the numbers of input and output units in the weight tensor, respectively. The neuron biases in dense layers is initialized with the constant 0. The rectified linear units in our multilayer perceptron are provided positive inputs to accelerate the early stages of learning.

III. RESULTS AND ANALYSIS

A. Data Collection

A series of radio propagation measurements at the *Q*-band (39.402 GHz) in Chilbolton are carried out using the Aldo Paradoni Payload propagation beacon [20]. The weather condition data are collected by the Chilbolton Facility for Atmospheric and Radio Research Campbell Scientific PWS100, the present weather sensor in Chilbolton. The instrument is mounted approximately 10 m above the ground on the roof of a cabin at the Chilbolton Observatory site. We take the radio propagation measurement data and weather condition data from January 1 to December 31, 2017. For the tradeoff between accuracy and complexity, the received signal and parameters of weather conditions are sampled by 1/60 Hz. The excess attenuation is calculated based on the received signal [20].

B. Comparison in the Time Domain

In Fig. 3(a), a total of 3000 samples of measurement data and predicted data by input vectors X_1, X_2, X_3, and X_4, are shown. As can be observed, the predicted data follow well the trends of the channel excess attenuation, thus qualitatively confirming the prediction ability of the proposed method.

Fig. 3(b), which is a zoom-in version of the selected red part of Fig. 3(a), compares the performance when the four different input vectors are used. There are 12 significant peaks, which are meaningful to be predicted in the 150 samples shown in Fig. 3(b). The prediction by input vectors X_2 and X_4, which has the channel excess attenuation in the previous 1 min as the input vector, can predict all 12 peaks in 150 samples. The prediction by input vectors X_1 and X_3, which only has the weather conditions as input vector, cannot predict the variation of channel extenuation at peaks 5–7. Moreover, the predictions by input vectors X_1 and X_3 at peaks 4, 8, and 10 are lower than the measurement data, not as accurate as those obtained from input vectors X_2 and X_4.

C. Statistical Analysis

In order to quantify the performance of the proposed method, next, we present statistical analysis of the predicted results versus the actual measured results. The means, standard deviations, and Pearson product–moment correlation coefficient (PCC) between the measurement data and the predicted data are given in Table II. The means of the predicted data by four different input vectors are roughly equal with the mean of the measurement data. However, their standard deviations show some significant statistical differences. The standard deviations of predictions by input vectors X_2 and X_4, which have the channel excess attenuation in the previous 1 min as an input vector, are closer with that of the measurement data. The PCC between the measurement

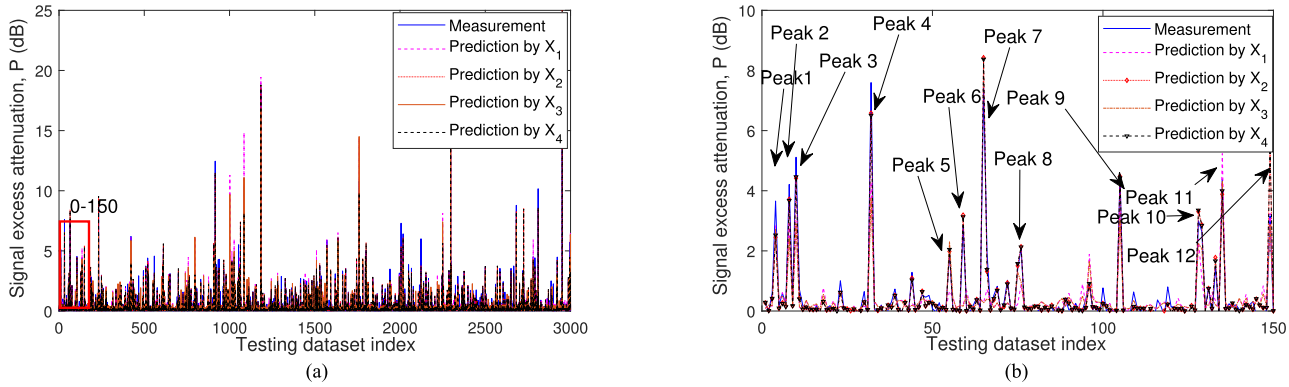

Fig. 3. Time series of measurement data and predicted data by X_1, X_2, X_3, and X_4. (a) 3000 samples of the measurement data and the predicted data. (b) 150 samples of the measurement data and the predicted data.

TABLE II
MEANS, STANDARD DEVIATIONS, AND PCC BETWEEN MEASUREMENT DATA AND PREDICTED DATA BY X_1, X_2, X_3, AND X_4

Statistics \ Input Vector	Measurement	X1	X2	X3	X4
Mean	0.4041	0.4007	0.4079	0.4028	0.412
Standard Deviation	1.2338	0.9477	1.211	0.914	1.2075
Correlation Coefficient	1	0.761	0.9549	0.7696	0.9549

TABLE III
MSES OF PREDICTED DATA BY X_1, X_2, X_3, AND X_4 IN THREE SETS

Data Set \ Input Vector	X_1	X_2	X_3	X_4
Train Set	0.6734	0.1601	0.6464	0.1594
Validation Set	0.7206	0.1558	0.6938	0.1566
Test Set	0.6407	0.1352	0.6219	0.1352

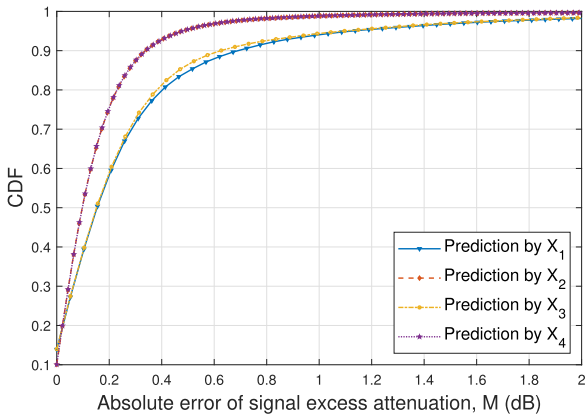

Fig. 4. CDFs of the absolute error of predicted data by X_1, X_2, X_3, and X_4.

data and the predicted data by input vectors X_2 and X_4 are both 0.9549, nearly to 1, which shows their effectiveness. Instead, the PCC between the measurement data and the predicted data by input vectors X_1 and X_3 are much lower.

The MSEs of the predicted data for the train set, validation set, and test set are presented in Table III. The MSE trends in the three datasets are relatively stable, which demonstrate the validation and stationarity of our ANN. The MSEs of predictions by input vectors X_2 and X_4 are much lower than those of predictions by input vectors X_1 and X_3. The cumulative distribution functions (CDFs) of the absolute error of the predicted data against the measured ones are shown in Fig. 4. Compared with predictions by input vectors X_1 and X_3, the CDFs of the absolute error of the predicted data by X_2 and X_4 are much higher and with a faster rise. The percentages of the absolute error within 1 dB by both X_1 and X_3 are above 90%. Adding the channel attenuation in the previous 1 min as input (X_2 and X_4), the percentage of the absolute error within 1 dB is 98.85%. The CDF of the absolute error of the predicted data by X_1 is very similar to the CDF of the absolute error of the predicted data by X_3, which suggests that the additional weather data associated with a disdrometer are not particularly helpful for predicting the fading.

IV. CONCLUSION

In this letter, we have proposed a method of estimating channel excess attenuation in mmW satellite links using the ANN. The data used to train the ANN were obtained by measurement campaigns of local weather conditions and the satellite communication signal by the Alphasat beacon receiver at the Q-band in Chilbolton. By analyzing time series as well as statistical characteristics obtained by the proposed ANN against the measured data, we have demonstrated that it is possible to obtain very accurate estimations of the channel excess attenuation using information obtained from low-cost weather instrumentation and CSI from the return link. Especially, the CDF of the absolute error between the ANN estimation and the measurement within a 1 dB range has already exceeded 98.8%. We also found that predictions that have the channel excess attenuation in last minute as the input vector can obtain much better performance, while predictions that have two more parameters of weather information as the input vector can only obtain slightly better performance. The proposed methodology can, thus, provide pertinent pathways for the efficient and low-cost deployment of propagation impairment mitigation techniques, such as adaptive coding and modulation and dynamic power control.

REFERENCES

[1] *Study on New Radio (NR) to Support Non Terrestrial Networks*, 3GPP, TR 38.811, Dec. 2017.

[2] H. Fenech, A. Tomatis, S. Amos, J. S. Merino, and V. Soumpholphakdy, "An operator's perspective on propagation," in *Proc. 8th Eur. Conf. Antennas Propag.*, The Hague, The Netherlands, Apr. 2014, pp. 2164–3342.

[3] *Digital Video Broadcasting (DVB); Second Generation Framing Structure, Channel Coding and Modulation Systems for Broadcasting, Interactive Services, News Gathering and Other Broadband Satellite Applications; Part 2: DVB Extensions (DVB-S2X)*, ETSI EN 302 307-2 v1.1.1, Oct. 2014.

[4] E. Casini, R. De Gaudenzi, and A. Ginesi, "DVB-S2 modem algorithms design and performance over typical satellite channels," *Int. J. Satell. Commun. Netw.*, vol. 22, pp. 281–318, Jun. 2004.

[5] G. Karam and H. Sari, "A data pre-distortion technique with memory for QAM radio systems," *IEEE Trans. Commun.*, vol. 39 no. 2, pp. 336–344, Feb. 1991.

[6] B. Li, C. Zhao, M. Sun, H. Zhang, Z. Zhou, and A. Nallanathan, "A Bayesian approach for nonlinear equalization and signal detection in millimeter-wave communications," *IEEE Trans. Wireless Commun.*, vol. 14, no. 7, pp. 3794–3809, Jul. 2015.

[7] *Calculation of Free-Space Attenuation*, ITU-R P.525-3, Sep. 2016.

[8] *Attenuation by Atmospheric Gases*, ITU-R P.676-11, Sep. 2016.

[9] *Characteristics of Precipitation for Propagation Modelling*, ITU-R P.838-7, Jun. 2017.

[10] *Attenuation Due to Clouds and Fog*, ITU-R P.840-7, Dec. 2017.

[11] Z. Qu, G. Zhang, H. Cao, and J. Xie, "Stochastic dynamic modeling of rain attenuation: A survey," *China Commun.*, vol. 15, no. 3, pp. 220–35, Mar. 2018.

[12] W. Vogel and J. Goldhirsh, "Earth-satellite tree attenuation at 20 GHz: Foliage effects," *Electron. Lett.*, vol. 29, no. 18, pp. 1640–1641, Sep. 1993.

[13] E. Cid, A. V. Alejos, and M. G. Sanchez, "Signaling through scattered vegetation: Empirical loss modeling for low elevation angle satellite paths obstructed by isolated thin trees," *IEEE Trans. Veh. Technol. Mag.*, vol. 11, no. 3, pp. 22–28, Sep. 2016.

[14] C. Loo, "Statistical models for land mobile and fixed satellite communications at Ka band," in *Proc. Veh. Technol. Conf.*, Atlanta, GA, USA, Apr. 1996, pp. 1023–1027.

[15] H.-P. Lin, R. Akturan, and W. J. Vogel, "Photogrammetric satellite PCS channel modeling using Markov chain approach," in *Proc. IEEE Int. Conf. Commun.*, Dallas, TX, USA, Jun. 1996, pp. 1735–1739.

[16] C.-X. Wang, J. Bian, J. Sun, W. Zhang, and M. Zhang, "A survey of 5G channel measurements and models," *IEEE Commun. Surv. Tut.*, vol. 20, no. 4, pp. 3142–168, 4th Quart. 2018.

[17] S. Wu, C.-X. Wang, H. Aggoune, M. M. Alwakeel, and X. You, "A general 3D non-stationary 5G wireless channel model," *IEEE Trans. Commun.*, vol. 66, no. 7, pp. 3065–3078, Jul. 2018.

[18] L. Bai *et al.*, "Predicting wireless mmWave massive MIMO channel characteristics using machine learning algorithms," *Wireless Commun. Mobile Comput.*, vol. 2018, Aug. 2018, Art. no. ID 9783863.

[19] J. Huang *et al.*, "A big data enabled channel model for 5G wireless communication systems," *IEEE Trans. Big Data*, 2019, to be published, doi: 10.1109/TBDATA.2018.2884489.

[20] S. Ventouras *et al.*, "Large scale assessment of Ka/Q band atmospheric channel across Europe with ALPHASAT TDP5: The augmented network," in *Proc. IEEE Eur. Conf. Antennas Propag.*, Paris, France, Mar. 2017, pp. 1471–1475.

[21] Keras Document, 2015. [Online]. Available: https://keras.io/

[22] S. Ruder, "An overview of gradient descent optimization algorithms," 2016, *arXiv:1609.04747v2*.

[23] X. Glorot and Y. Bengio, "Understanding the difficulty of training deep feedforward neural networks," *J. Mach. Learn. Res.*, vol. 9, pp. 249–256, 2010.